

# Charge Transfer Noise and Lag in CMOS Active Pixel Sensors

Eric R. Fossum, *Fellow Member IEEE*

## Abstract

This paper reports on the investigation of charge-transfer noise and lag in CMOS image sensors. Noise and lag are analyzed for buried-photodiode CMOS active-pixel-sensor (APS) devices using a simple Monte-Carlo technique. Since the main mechanism of charge-transfer noise involves carrier emission over a barrier, the results are applicable to the soft reset of photodiode-type CMOS APS devices, and charge transfer from a single-poly-photogate-type CMOS APS with a bridging diffusion. Whereas the literature and conventional wisdom has focused on either  $(kTC)^{1/2}$  or  $(kTC/2)^{1/2}$  like behavior, the noise is found to behave like shot noise for both small and large signals.

## I. Introduction

Noise related to the incomplete transfer of charge has been studied almost since the invention of the charge-coupled device (CCD) and its less famous cousin, the bucket-bridgade device (BBD) [1-3]. In Thornber's 1974 seminal paper [4], he described numerous noise sources related to charge transfer and their associated effect on the total noise in a charge transfer device. In modern CCDs, however, noise is dominated by either signal chain noise for low-light-level illumination, or by photon shot noise for brighter illumination.

The advent of CMOS active pixel sensors was precipitated by the desire to avoid the thousands of charge transfers inherent in a CCD and the need for high charge transfer efficiency (CTE). This is because a high CTE requirement in turn sets undesirable requirements for semiconductor device structures, fabrication processes and operating voltages. These shortcomings, particularly in fabrication processes (compatibility with on-chip analog and digital circuitry) and power dissipation, are overcome in state of the art CMOS image sensors [5].

In state of the art CMOS APS devices, at least one charge transfer is usually required in the readout process. For a four-transistor (4T) buried-photodiode (or pinned-photodiode) device [6], charge must be transferred from the buried photodiode to a

floating sense node. In a photogate device [7,8] charge must be transferred from a deep-depleted MOS potential well to a floating sense node. In a three-transistor (3T) photodiode-type device, charge must be transferred from the photodiode to a reset drain in order to generate the output signal [9,10]. While high CCD-like charge transfer efficiency is not required, incomplete transfer of charge can lead to noise and lag.

Charge transfer noise and lag in 3T devices has been studied by JPL [11] and Stanford [12]. Generally the reset operation in 3T CMOS APS devices is termed either “hard reset” or “soft reset”. Hard reset refers to the reset transistor in strong inversion so that the photodiode and reset drain are in thermal equilibrium. Turning the reset gate off leads to a variance in voltage on the photodiode  $\sigma_{V_{pd}}^2$  given by:

$$\sigma_{V_{pd}}^2 = kT/C \quad (1)$$

where  $k$  is Boltzmann’s constant,  $T$  is temperature and  $C$  is the capacitance of the photodiode. This is referred to as  $kTC$  noise. A representative value of  $C$  is 5 fF making  $\sqrt{\sigma_{V_{pd}}^2}$  approximately 900  $\mu$ V rms. Noise is often expressed in electrons  $N$ , leading to a variance in number of electrons  $\sigma_N^2$  given by:

$$\sigma_N^2 = kTC / q^2 \quad (2)$$

which has a value of 28 e- rms for the case above.

Soft reset refers to a situation where the reset transistor is operating in the (deep) subthreshold regime at the end of the reset period. This situation arises from the combination of the applied reset gate voltage and reset drain voltage. Often the reset gate “on” voltage and the drain voltage are both  $V_{dd}$  and this leads to soft reset. Under soft reset, the photodiode and the reset drain do not reach thermal equilibrium. Carriers are emitted from the photodiode, over the effective barrier under the reset gate to the reset drain.

Generally it is held that soft reset leads to a noise that is reduced by a factor of  $\sqrt{2}$  from the  $kTC$  noise level. The simplest explanation is that unlike hard reset where electrons can move bi-directionally under Brownian motion either to or from the photodiode, in soft reset the electrons can only appreciably move uni-directionally from the photodiode to the reset drain and hence the factor of 1/2 in the variance. (The author

first heard this explanation from the late Walter Kosonocky a long time ago and similar arguments appear in the literature from JPL and Stanford.) However, according to the analysis by Thornber, the noise reduction factor may be slightly larger than 2 and this is not as intuitively satisfying. We will return to soft-reset noise in a later section.

In 4T CMOS APS devices utilizing buried photodiodes, complete transfer from the buried photodiode is sought so that the pixel's contribution to read noise, through the use of correlated double sampling (CDS), can effectively be zero. In the 4T device, the floating sense node is first reset and this reset voltage measured. The signal charge is then transferred from the buried photodiode to the sense node, and the sense node voltage measured a second time. The difference in these two voltages is equal to the ratio of the transferred charge to the sense node capacitance. Noise in the transferred charge cannot be suppressed using CDS.

To date few papers discussing performance of 4T CMOS APS devices report an associated image lag, though in private communication some lag is acknowledged. Albeit small, the presence of lag suggests that transfer of charge from the buried photodiode was not complete. An issue to be addressed in this paper is the impact on pixel read noise for incomplete charge transfer. Since several parallels can be drawn between soft reset in a 3T CMOS APS and the barrier-induced incomplete transfer in a 4T buried photodiode device, the expectation is that the noise varies like  $(kTC/2)^{1/2}$ . We find that this is not the case and that the noise is better approximated by  $N_{\text{sig}}^{1/2}$ , where  $N_{\text{sig}}$  is the number of signal carriers successfully transferred from the buried photodiode.

## II. Ideal Carrier Emission

Consider the simple case of a carriers being emitted from a potential well over a barrier of total height  $\phi_b$  volts, as shown in Fig. 1.

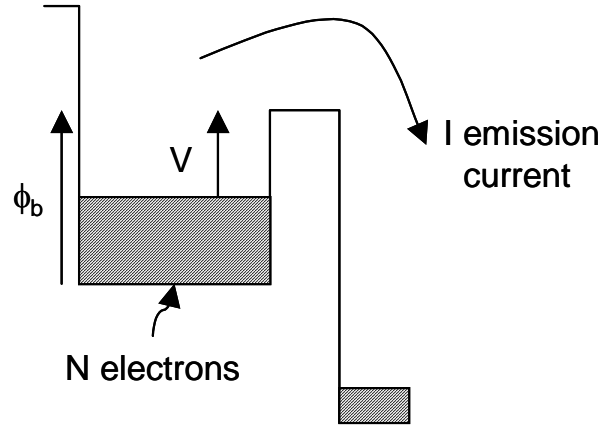


Figure 1. Carrier emission from a potential well over a barrier with height  $V$ .

If the well is filled with  $N$  electrons, and the well capacitance given by  $C$ , then the barrier seen by electrons  $V$  is given by:

$$V = \phi_b - qN/C \quad (3)$$

where  $N \leq C\phi_b/q$ . The emission rate of electrons from the well, across the barrier, is proportional to the number of carriers with energy greater than the barrier. The number of electrons at the same or greater energy than the barrier is the product of the Fermi distribution and the number of states (with the right momentum), integrated from the barrier energy level and up. Note that the density of states for energy less than the barrier energy level is relatively irrelevant, so we need not concern ourselves with the other details of the potential well.

The resultant emission current,  $I$ , can be approximately written as:

$$I = I_0 e^{-\beta V} \quad (4)$$

where  $\beta = q/mkT$ ,  $m$  is the so-called ideality factor, and  $I_0$  depends on numerous physical and material constants.  $I$  is taken as a positive quantity for simplicity.  $I_0$  can also be obtained from fitted MOSFET subthreshold models.

The voltage  $V$  varies in time due to the discharge of carriers, and is simply

$$V(t) = V_o - qN_e(t)/C \quad (5)$$

where  $N_e(t)$  is the total number of emitted carriers over the barrier and  $V_o = V(t=0)$ . We also have:

$$dV/dt = I/C \quad (6).$$

Combining equations 4,5, and 6 leads to a differential equation for  $V(t)$  whose well-known solution is:

$$V(t) = (1/\beta) \ln [ (I_o\beta/C) t + e^{\beta V_o} ] \quad (7)$$

Equation 7 shows that the potential barrier for carriers grows logarithmically in time with a time scale factor proportional to  $I_o$  and  $1/C$ .

In the case of a finite well (that is, the number of carriers in the well such that in the time frames of interest, all the carriers may be emitted) the time to discharge the well is given by solving equation 7. We obtain the discharge time  $\tau_d$  as:

$$\tau_d = [ e^{\beta\phi_b} - e^{\beta V_o} ] C/\beta I_o \quad (8)$$

Taking  $V_o = 0$ ,  $\phi_b = 0.2V$ ,  $C = 5$  fF, and  $I_o = 100$  nA, we obtain a discharge time of 3  $\mu$ sec. However, increasing  $\phi_b$  to 1.0V increases the discharge time to about 2-1/2 years. In practice, though, such a well would soon reach steady state so that the emission rate of carriers out of the well would be replenished at an equal rate by thermal and/or optical generation of carriers in the vicinity of the well. For example, if the well generation rate is 10 carriers/sec, in under 10 seconds the barrier  $V$  would reach a steady-state value of about 0.64 volts.

It is interesting to note that for a finite well, the discharge current cuts off suddenly when the potential well becomes empty of carriers. For infinite wells (an infinite well is the opposite of a finite well), the discharge current continues indefinitely at a continually decreasing level. This indefinite discharge period has always been one of the major problems with lag in an image sensor in that it is persistent. For finite wells though, lag can be eliminated if sufficient time is allotted for the discharge.

We also note that the discharge process can be interrupted by suddenly increasing the size of the barrier (e.g. by turning off a MOSFET gate), and then resumed once the barrier is restored to its earlier value.

Noise in the emission process has been treated in the references cited above. JPL shows that the variance  $\sigma_e^2$  in the number of emitted carriers  $N_e$  is given by:

$$\sigma_e^2 = \xi [1 - e^{-N_e/\xi}] \quad (8)$$

where  $\xi = C/2\beta q = mkTC/2q^2$ . For  $m = 1$  and  $C = 5\text{fF}$ ,  $\xi \cong 400$ . For a small number of emitted carriers equation 8 reduces to:

$$\sigma_e^2 \cong N_e \quad \text{for } N_e \ll \xi \quad (9)$$

and for a large number of emitted carriers equation 8 reduces to:

$$\sigma_e^2 \cong mkTC/2q^2 \quad \text{for } N_e \gg \xi \quad (10)$$

This means that the noise for a small number of emitted carriers looks like shot noise, and the noise for a large number of emitted carriers goes like  $[kTC/2]^{1/2}$ .

This is an interesting result and is due to the feedback of the barrier height growth as carriers are emitted. If the barrier height did not grow, the noise in total emitted carrier count would look like shot noise (i.e., vary as the square root of the total number of emitted carriers) but the feedback forces the noise to become  $kTC$ -like. It also suggests that even if the initial noise, or uncertainty in the number of carriers is high, it will evolve back to  $kTC$ -like behavior. For large signals for example, in reset, the initial discharge of a 3T CMOS APS photodiode may be dominated by thermal conductance noise in the reset MOSFET, then evolve to  $kTC$  noise, and then once the reset MOSFET enters the subthreshold regime, the noise further reduces to equation 10. (This hard-to-soft reset noise reduction was described and experimentally confirmed by JPL [11]). Thus, the initial noise in the potential well is lost to memory and is not considered further in this paper.

It is here that one can make an erroneous assumption regarding noise in carriers emitted from a buried photodiode if the buried photodiode has a barrier leading to incomplete charge transfer. It is tempting to assume that if a few carriers are emitted

from the barrier, the noise will look shot-noise like, and if many carrier are emitted, the noise becomes kTC-like. This is not the case as described later.

### III. Simple Monte-Carlo Model

To examine noise processes for cases that do not exactly fit the JPL model and may not be easily analyzed using mathematical techniques, a simple Monte-Carlo type charge-control model or simulation was developed for spreadsheet operation. In the simulation, some initial number of electrons is assumed to be present in the potential well with total barrier  $\phi_b$  as described above. In some small time increment, a small number of carriers  $n_e$  are emitted according to equation 4, with the barrier height kept constant. The time increment depends on the time scaling factors  $I_0$  and  $C$  and was selected such that shorter time increments and somewhat larger time increments did not affect the outcome of the calculation.

#### IIIa. Discharge only

For a small number of emitted carriers  $n_e$ , we assume that the variance in  $n_e$  is given by  $\sigma_n^2$  such that

$$\sigma_n^2 = n_e \quad (11)$$

(This looks shot-noise like because this process is in fact the historical origin of shot noise). In the model the number of carriers emitted is reduced (or increased) by a random amount in accordance with this variance. (The exact technique used in the spreadsheet is described in Appendix A). The new number of carriers remaining in the potential well and a new barrier height is then calculated. The process is repeated hundreds of times for a total time interval  $T_r$ . At the end of this transient period or trial, there exists a certain number of electrons in the potential well, a certain number emitted  $N_e$ , and a barrier height  $V$ . If the transient is repeatedly calculated (using time varying random numbers in the calculation of the actual number of emitted carriers in each small time increment), then the outcome of a number of transient trials has a variance in both barrier height  $V$  and number of electrons emitted  $N_e$ . The number of transient trials performed affects the accuracy of the obtained variance relative to the outcome of an

analytical approach, and for calculation sanity, a certain inaccuracy in the variance is acceptable.

One can also calculate the variance across a number of transient trials after each small time increment, obtaining the variance in emitted carriers as a function of time or total number of emitted carriers. An example calculation is shown below in Figure 2 for  $C = 5$  fF.

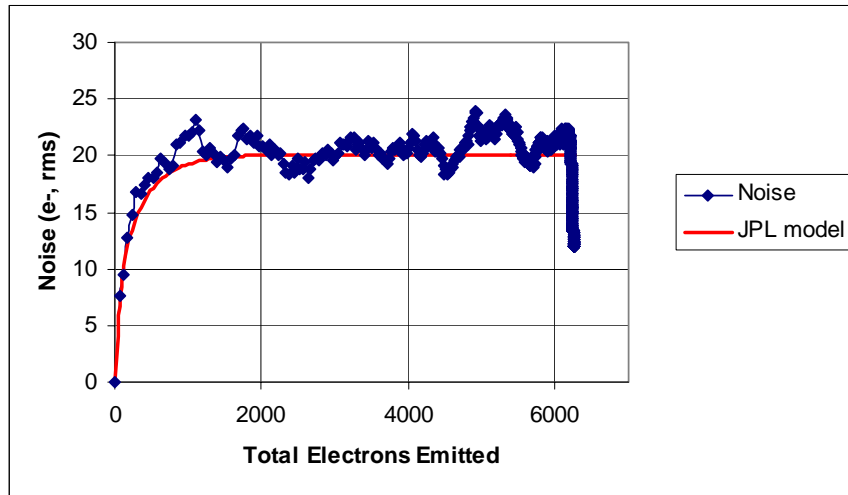


Figure 2a. Noise in emission of carriers from a simple potential well as a function of avg. total carriers emitted calculated by JPL analytical expression and by Monte-Carlo technique.

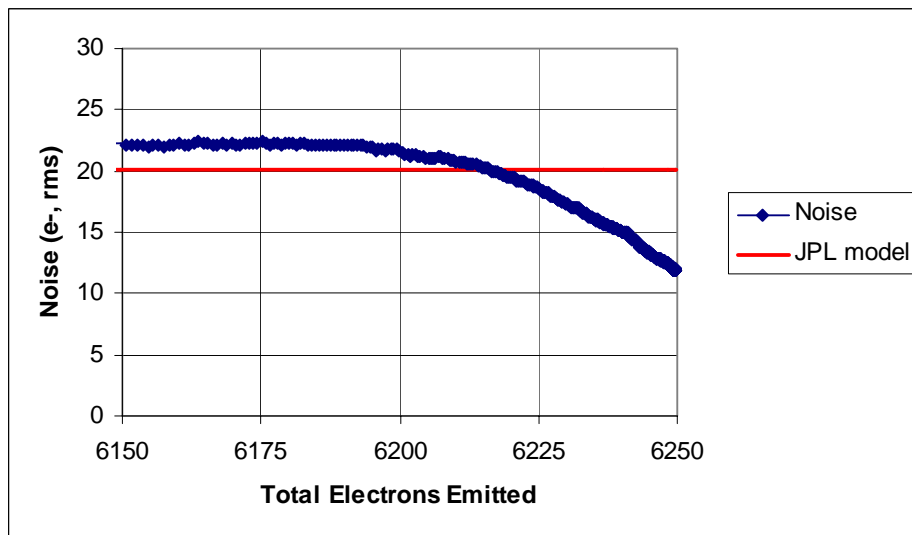


Figure 2b. Noise as a function of total electrons emitted for complete charge transfer. Note decrease in noise as well becomes emptied of electrons. (6,250 electrons in well).

For a capacitance of 5 fF, we expect  $(kTC/2)^{1/2}$  noise to have a value of about 20 electrons, r.m.s. As seen in Figure 2a, the Monte-Carlo simulation results tracks the JPL expression quite well giving us confidence in the Monte-Carlo calculations. This simulation was done for a finite well with about 6,250 electrons.

In Figure 2b we see that the Monte-Carlo model shows an abrupt decrease in noise once the average number of remaining electrons is approximately equal to twice the  $(kTC/2)^{1/2}$  noise level, and decreasing almost linearly to a value approximately equal to  $(1/2)(kTC/2)^{1/2}$  at “empty well” or after 6,250 electrons have been emitted, on the average. This is quite a reasonable result since the potential well will have emptied itself of electrons on some transient trials faster than other trials, and the spread in this is reflected in the variance in the number of carriers emitted. Once a well is empty, that transient trial’s contribution to the noise calculation becomes nil.

To examine the effect of equation 11 on noise it was modified to:

$$\sigma_n^2 = a n_e^z \quad (11a)$$

where constants a and z were varied. For example, setting a=0.1 and z=2 yields a noisy emission characterized by a standard deviation proportional to the number of carriers emitted. While there is no physical reason to believe the emission process obeys this description, it was easy to change in the simulation. It was found that a proportional noise relationship gave a noise that decreased linearly with the total number of emitted carriers rather than remaining constant at  $(kTC/2)^{1/2}$ . The constant a determined the initial noise magnitude and rate of decrease. On the other hand, taking a=1 and varying z such that  $2/3 \leq z \leq 3/2$  changed the noise so that it continued to remain constant with the total number of emitted carriers, like in Fig.2a, but with a value of  $(kTC/z_0)^{1/2}$ , where  $z_0 > 2$  for  $z < 1$ , and  $z_0 < 2$  for  $z > 1$

### IIIb. Optical input

In 4T CMOS APS buried-photodiode devices, and in 3T CMOS APS photodiode devices in soft reset, the potential well is filled with electrons via optical input. The Monte-Carlo model was modified to include the effect of photon shot noise. If the well should, on average, have  $N_i$  electrons added due to optical input, then the number of

electrons added was calculated to be  $N_i$  plus a random number of electrons where that random number had a probability distribution function with a mean of zero and a variance equal to  $N_i$ .

The following sequence was simulated. First, a packet of carriers of average value  $N_i$  and variance  $N_i$  was added to the potential well without any carriers being emitted. This corresponds, for example, to a 3T device photodiode or a 4T buried-photodiode device during integration where the reset or transfer gates are respectively

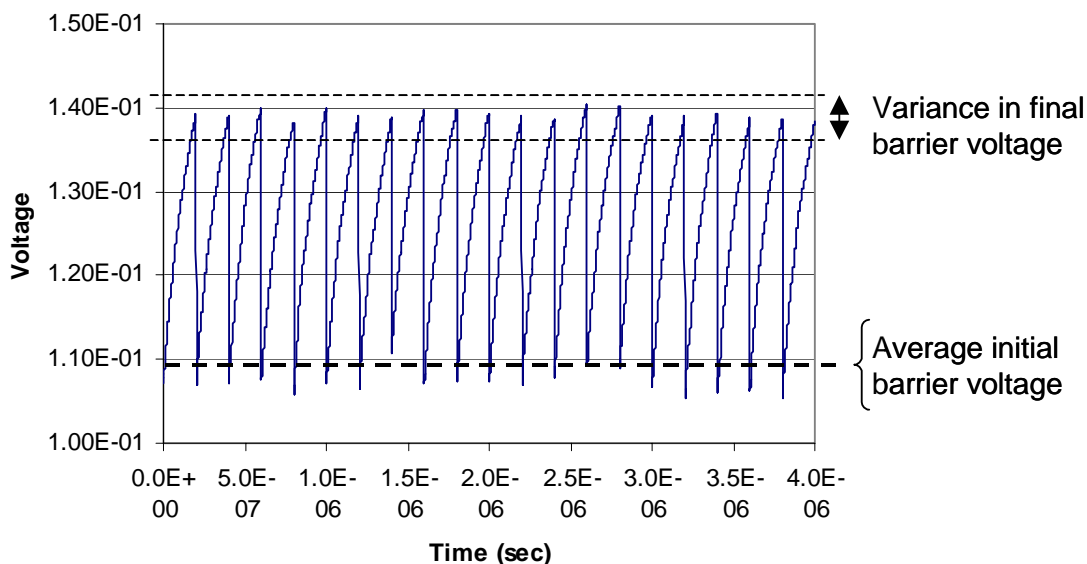


*Figure 3. Example of barrier voltage vs. time for 20 cycles of simulation of new optical input followed by emission of carriers over the barrier.*

turned “off”. Next, the carriers are emitted from the well for some period of time  $T_r$ . This corresponds to either the reset of a 3T photodiode pixel, or the transfer of charge from a buried photodiode. At the end of this reset or transfer interval a new optical input is added and the process repeated hundreds of times. A steady-state variance in emitted electrons per cycle, barrier voltage and number of carriers in the well is achieved. This variance represents the noise in the process. These cycles are shown Figure 3.

Before initiating this simulation sequence, it is helpful to calculate the steady-state average initial barrier voltage. This is the initial voltage where the subsequent average number of emitted electrons  $N_e$  over the cycle equals the average number of input electrons  $N_i$ . Determination of this average initial barrier voltage requires solution of a

transcendental equation. The solution is performed numerically in the spreadsheet and is used as a starting point for the subsequent transient simulation.

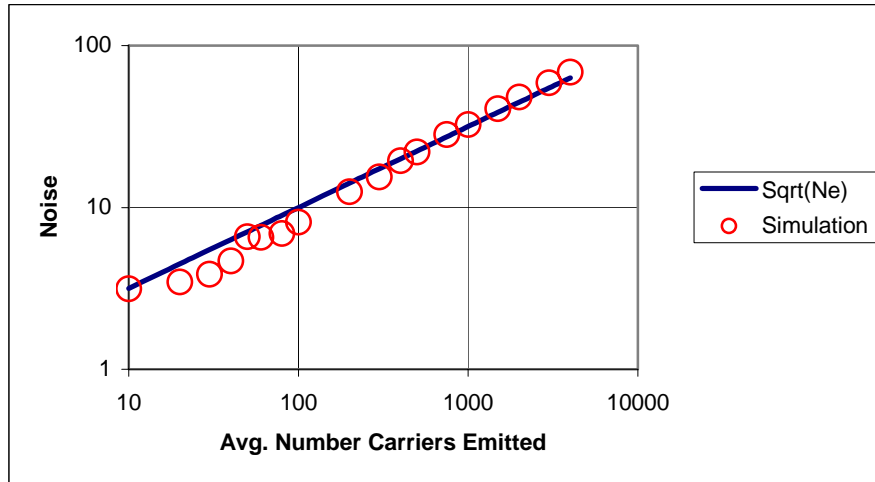


Figure 4. Noise as a function of average number carriers emitted for steady state optical input.

The results of several simulations are shown as an example in Figure 4 for  $I_0=100$  nA,  $C = 5$  fF, and  $T_r = 200$  nsec. By adjusting the average input signal  $N_i$ , the average number of carriers emitted  $N_e$  was varied from  $\xi/40 \leq N_e \leq 10\xi$ . It can be readily seen that the noise is best described as  $N_e^{1/2}$  and there is no region where the noise behaves as kTC-type noise. This is because at a small number of emitted carriers, the input photon shot noise and emission both contribute shot noise (yielding just shot noise) and at higher numbers of emitted carriers, the input photon shot noise dominates.

Thus, in a 3T photodiode-type CMOS APS, soft reset of the photodiode leads to shot-noise behavior in the pixel for all levels of optical input signal and low-noise results can be obtained under steady-state low-light-illumination conditions. This has been confirmed experimentally [13]. However lag will be an issue and this is addressed subsequently.

A 3T photodiode-type CMOS APS undergoing a hard reset will have the behavior described by JPL and Stanford. That is, for small signals the noise will be dominated by the  $(kTC)^{1/2}$  noise in the reset of the photodiode, or in the case of a hard-to-soft reset, by  $(kTC/2)^{1/2}$  noise. Both types of reset suppress lag, or at least the lag is manifested as a constant offset in all frames.

In a 4T buried-photodiode-type CMOS APS (or in a CCD with a buried photodiode), with no barrier and complete charge transfer achieved, pixel noise is determined by photon shot noise. Pixel noise will still be determined by photon shot noise even with a barrier causing incomplete charge transfer and lag.

In a 5T photogate-type CMOS APS with single poly and bridging diffusion, the bridging diffusion contributes lag, depending on its capacitance, but the output is photon-shot-noise limited.

#### **IV. Lag**

The Monte-Carlo simulation can be used to look at lag and noise. There are several physical mechanisms that can result in lag, including carriers diffusing from deep in the substrate towards the surface, or carriers being released from traps. In this paper we are only concerned with carriers being emitted from a finite or infinite potential well. The effect of this lag on a pixel's frame-by-frame output is similar to that of a low pass RC filter, where C is the capacitance of the well and R is large and related to the transfer (or reset) gate subthreshold conductance.

Potential-well-emission lag has directional behavior and has two types of responses. The first we call "discharging lag" which occurs when the light intensity is decreased suddenly from one frame to the next. This lag is characterized by a reduction in the number of carriers in the potential well in successive frames as the well discharges. The number of emitted carriers per frame also reduces. The second type of lag we call "charging lag" and occurs when the light level goes from a low level to a brighter level. In this case, the behavior is characterized by an increase in the number of carriers in the potential well and an increase in the number of carriers emitted from the potential well on each frame.

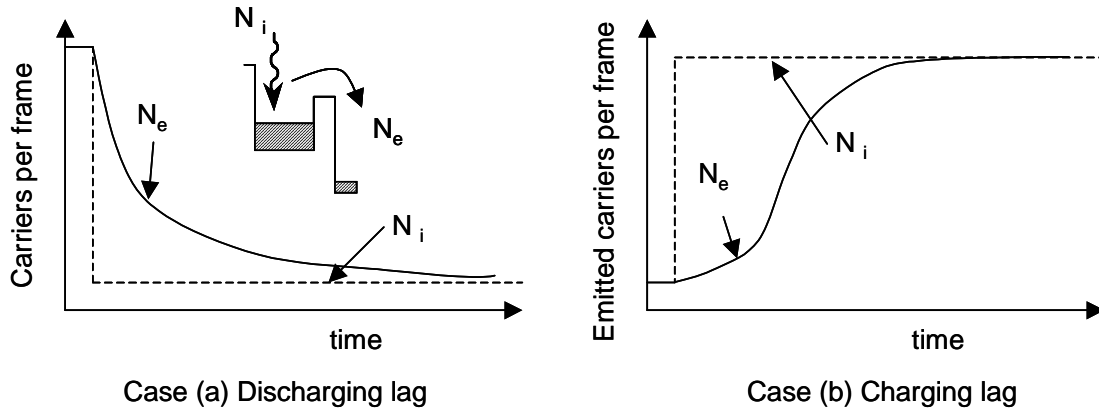


Figure 5. Two types of lag. Case (a) light is suddenly decreased to some low level. Case (b) light is suddenly increased from some low level. In each case the number of carriers in well adjusts so that emission rate  $N_e$  balances  $N_i$ .

#### IVa Discharging Lag

Discharging lag is the lag most familiar to image sensor and camera engineers and usually results in “comet tails” from bright lights in video images, or residual “ghost” images in still picture applications. If the input optical signal suddenly decreases, a new steady-state condition for the potential well must be achieved so that carriers are emitted from the well at a reduced rate commensurate with the optical input signal. In the simplest case, where the light is switched off at  $t=0$ , the average number of carriers that are emitted over the barrier from an infinite well in the time interval between  $t_2 > t_1 > 0$  and  $t_1 > 0$  can be determined from equation 7 as:

$$qN_e = C \{V(t_1) - V(t_2)\} = (1/\beta) \{ \ln [ ((I_0\beta/C) t_1 + e^{\beta V_0}) / ((I_0\beta/C) t_2 + e^{\beta V_0}) ] \} \quad (12)$$

We note that the discharge process may be divided across several frames so that if in each frame the reset or transfer time is  $T_r$ , then the time interval  $t_2 - t_1$  corresponds to  $N_f$  frames, where  $N_f = (t_2 - t_1) / T_r$ .

In a practical sense, the lag period, or “persistence”, can be considered complete when the optically-generated and dark current refilling the well during the integration period  $N_i$  is equal to the number of emitted carriers in the reset of a given frame  $N_e$ . A very rough estimate of the number of frames in the persistence from an infinite well can

be obtained by taking the potential well barrier voltage  $V$  to be approximately constant during the reset interval (assuming  $N_e$  is small) and setting  $N_i$  equal to  $N_e$ . The result for the number of frames  $N_f$  is given by:

$$N_f \cong 2 (C/I_o\beta T_r) [ (I_o T_r/qN_i) - e^{\beta V_o} ] \quad (13)$$

where the factor 2 makes equation 13 fit better with empirical results. For example, with  $C = 5$  fF,  $T_r = 200$  nsec,  $N_i = 10$  e-/sec, and the initial  $V_o$  corresponding to 1000 e-/sec, the persistence is approximately 160 frames.

In the case of a finite well, the persistence is bounded by the discharge time  $\tau_d$  as was shown in equation 9.

#### IVb. Charging Lag

Charging lag is familiar to many engineers who have worked with 3T photodiode CMOS APS devices under low light conditions with soft reset. In this case, the charging lag manifests itself as a “dead zone” when sweeping the photo response curve. Charging lag is generally less objectionable for video but can be of special concern for digital still camera applications where the pixel is held in reset for a long period prior to exposure to illumination. This can result in an image being partially swallowed up by the charging process and weakly illuminated portions of the image lost to black.

To estimate the charging time, we assume that prior to increasing the illumination, the photodiode has reached some steady state condition in the dark or low light where the barrier  $V$  is relatively large. Several frames worth of photogenerated signal may be required to recharge the potential well to the new steady-state condition commensurate with the new illumination level. If one assumes that all the new carriers go into charging the potential well, then one can obtain the approximate result that if the initial optical signal (including dark current) is  $N_1$  carriers/frame and the new signal is  $N_2$  carriers/frame, then the number of frames  $N_f$  required to charge the potential well is approximately:

$$N_f \cong (2C/q\beta N_2) \ln (N_2/N_1) \quad (14)$$

The factor of 2 makes equation 14 match better with empirical results since optically generated carriers near the end of the charging time are also lost to emission. For

example, with  $C = 5$  fF,  $N_1 = 10$  e-/frame and  $N_2 = 1000$  e-/frame then the charging time becomes about 7 frames.

#### IVb. Lag Noise

While the charging and discharging lag phenomena can be considered a type of image sensor noise, the lag transient contains temporal noise. Using the Monte-Carlo model described above, noise in charging and discharging lag was simulated. For discharging lag (brighter light to low light), the noise behaves similar to that predicted by the JPL model. That is, frame zero is dominated by photon shot noise, but the initial lag carrier emission appears more kTC-noise like, and once the number of emitted carriers declines, the noise varies as  $(N_e)^{1/2}$ . For charging lag (low light to brighter light), the simulated noise seems to vary as  $(N_e)^{1/2}$  as might be expected since for low numbers of emitted carriers, the noise contains both photon shot noise and emission shot noise. For larger numbers of carriers, the noise is dominated by the photon shot noise.

### **V. Conclusions**

A simple Monte-Carlo simulation was developed to better understand noise due to incomplete charge transfer in CMOS active pixel sensor (APS) devices. It was found that the pixel's output under steady-state illumination can be photon-shot-noise limited even in the presence of incomplete charge transfer. The penalty for incomplete charge transfer is lag. The lag transient was examined and lag time response scales directly with the capacitance. The transient's temporal noise will also look like shot noise.

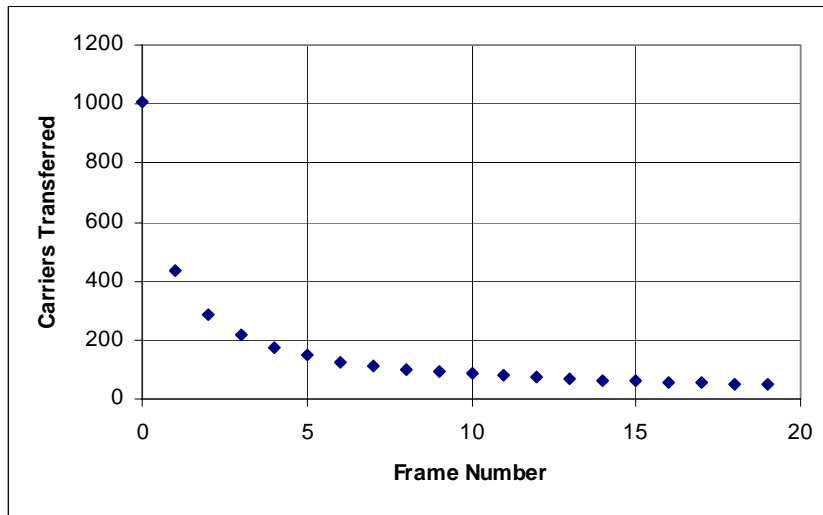


Fig 3a. Discharging lag for 1000 e-/frame initial illumination to 10 e-/frame for conditions in text. Note that lag transient continues for over 100 additional frames not shown for this case.

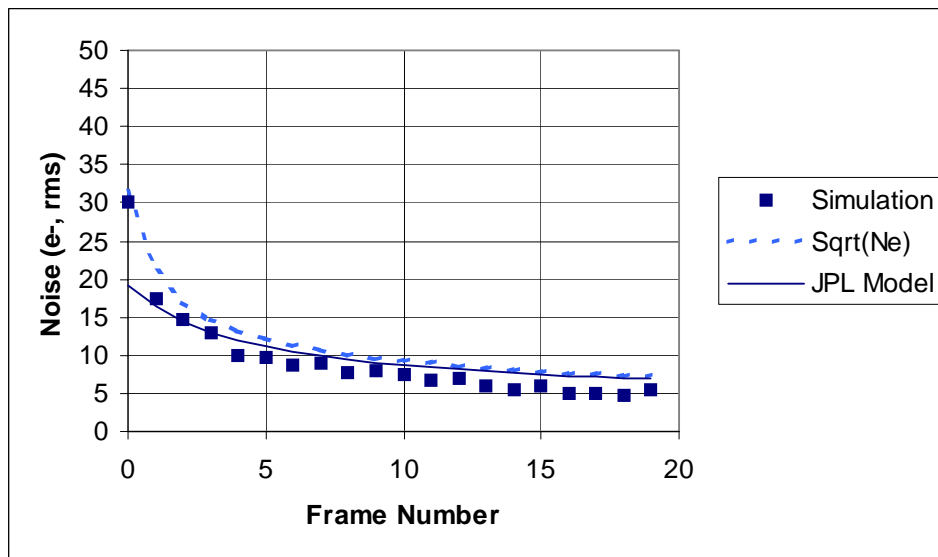


Fig 3b. Noise in discharging lag as a function of frame number. Also shown is the square root of the number of emitted electrons per frame, and the JPL noise estimate.

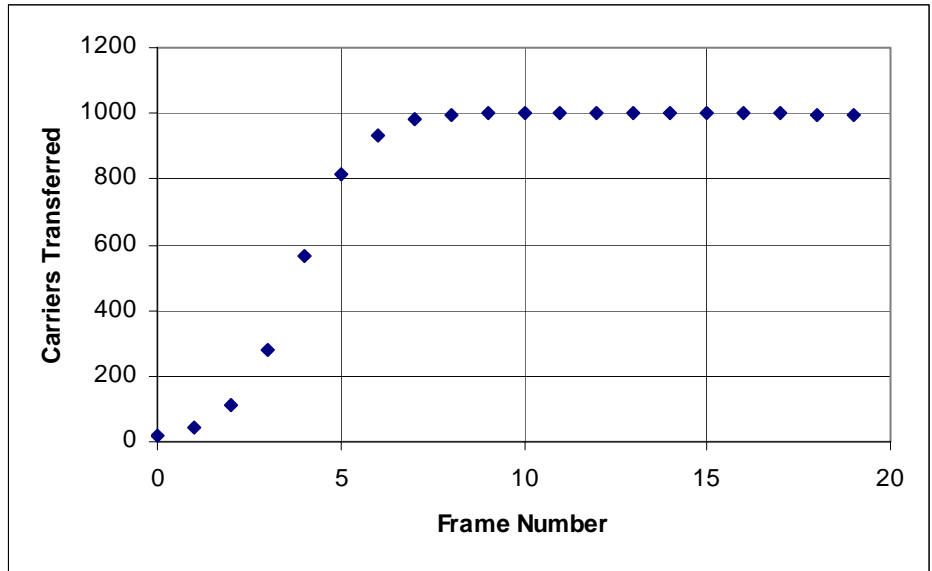


Fig 4a. Charging lag for initial illumination of 10 e-/frame increased to 1000 e-/frame, as a function of frame number for conditions in text. Note several frames of “dead output” before proper signal is restored.

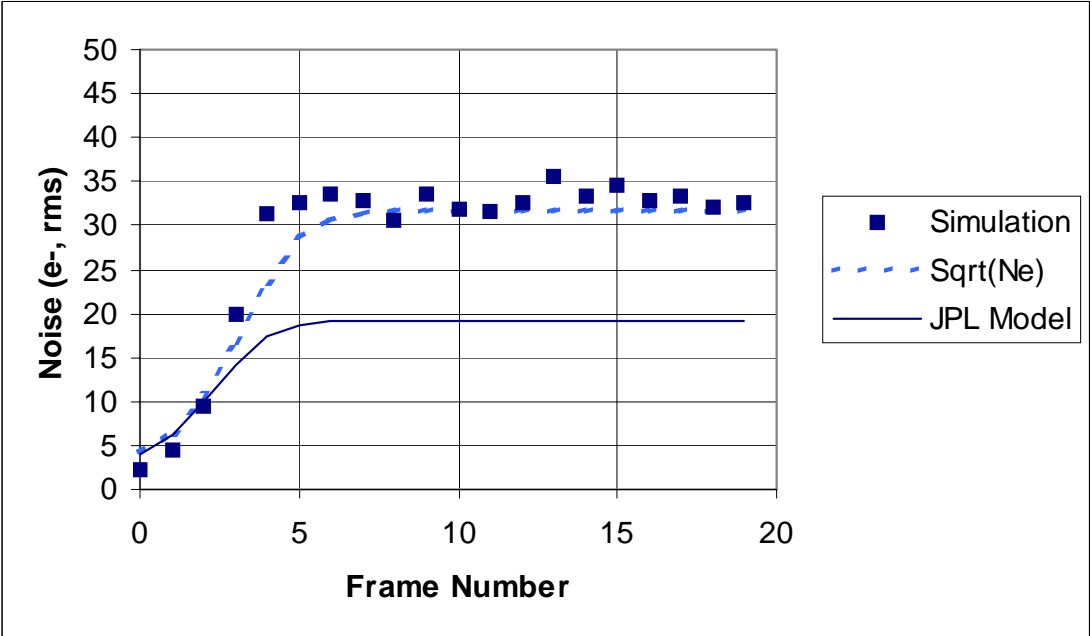


Fig 4b. Noise in charging lag as a function of frame number. Also shown is the square root of the number of emitted electrons per frame, and the JPL noise estimate.

## Appendix A Creating a random number with a defined distribution

Most random number generators generate a number between 0 and 1 with uniform probability distribution function  $p(x) = 1$  for  $0 < x < 1$  where  $p(x)$  is the probability of the random number generator returning the value  $x$ . For Monte-Carlo noise simulations, we will generally desire a normal probability distribution function where:

$$p(x) \sim \exp[-(x/\sigma)^2]$$

If we want a non-uniform distribution, like the normal distribution, then we need to find the transformation  $y = f(x)$  such that  $p(y)$  has the desired distribution for  $0 < x < 1$ .

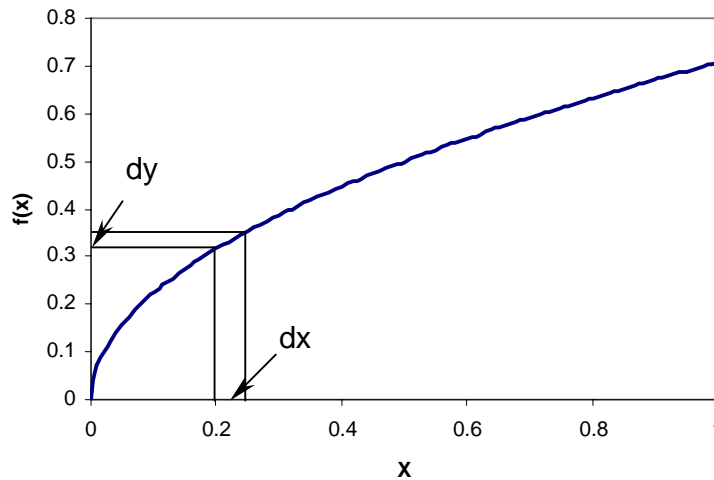


Figure A1. Example of transformation  $y = f(x)$ .

For example, suppose  $f(x) = (x/2)^{1/2}$  as shown in Fig A1 above. Consider the region  $dx$  and  $dy$  as shown. The probability of  $x$  being selected such that it falls in this region is  $p(x) dx$ . The probability of  $y = f(x)$  being in the region  $dy$  is equal to the probability of  $x$  being in region  $dx$ . That is, we have

$$p(y) dy = p(x) dx \text{ or}$$

$$p(y) = p(x) dx/dy, \text{ or finally, since } p(x) = 1,$$

$$p(y) = dx/dy.$$

Thus, in the example we have  $x = y^2/2$  and  $dx/dy = y$ . Thus,  $p(y) = y$  and the probability distribution is a linear ramp from  $y = 0$  ( $x=0$ ) to  $y=(1/2)^{1/2}$  ( $x=1$ ). This is shown in Fig.

A2 where EXCEL was used to calculate 1000 random numbers, where each number was set according to  $[2*\text{RAND()}]^{(1/2)}$ . A histogram is plotted comparing the generated distribution to the theoretical distribution. Note that each time the EXCEL worksheet is recalculated, a slightly different distribution is generated.

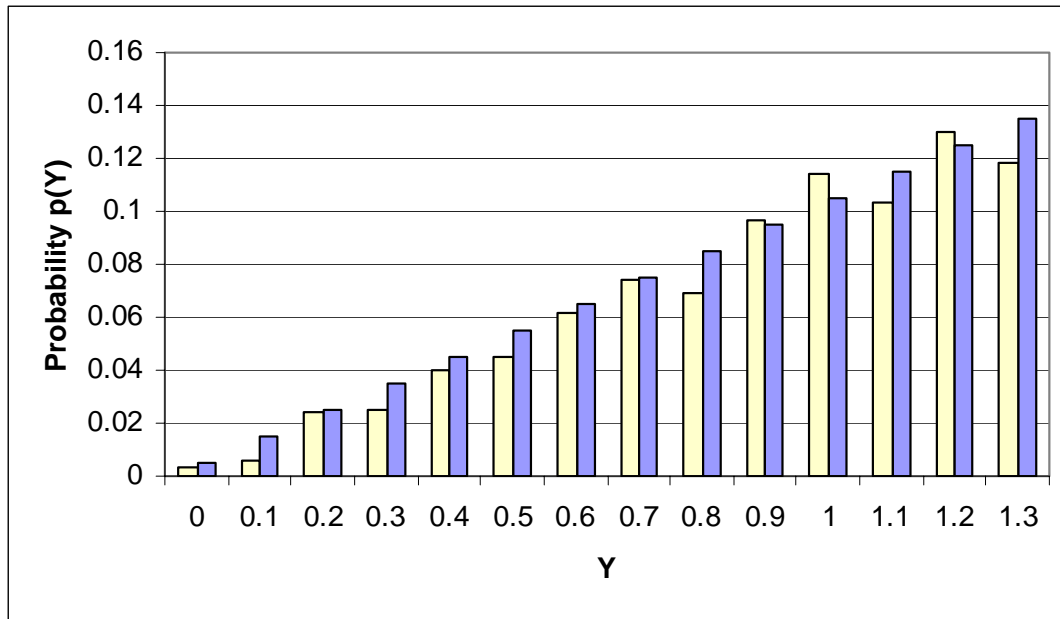


Figure A2. Linear probability distribution function generated by the transformation  $y = x(2)1/2$ . Yellow is the probability distribution from 1000 trials, and blue is the theoretical probability distribution.

This distribution can be readily transformed into a symmetric triangular distribution by changing the formula to:  $\{[\text{RAND()}]^{(1/2)}-1\} * \text{SIGN}(\text{RAND()}-0.5)$ . First the distribution is scaled to the range (0,1) by omitting the factor of 2, and then it is shifted to the left by value 1, and then ‘symmetrized’ by multiplying by a random number which is either +1 or -1. The result is shown in Fig A3 and it has a standard deviation of approximately 0.4 and a mean of zero.

Generally it is harder to work backwards to find  $f(x)$ . For example, suppose we want  $p(y) = y^2$ . We must solve  $dx/dy = y^2$ . Integrating we get  $x = y^3/3$  and solving for  $y$  we get  $y = (3x)^{1/3}$ .

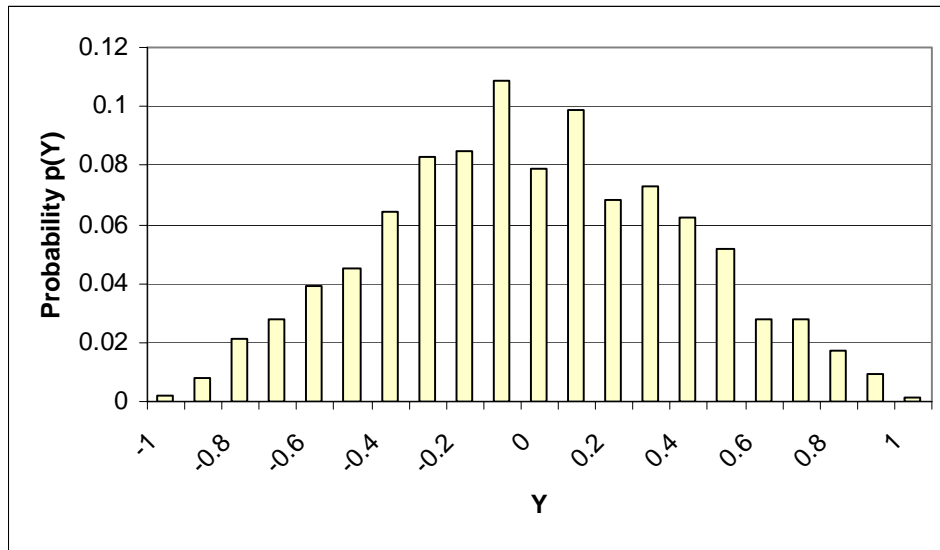


Figure A3. Triangular probability distribution function generated from 1000 trials as described in text.

In EXCEL, for example, one would then set a cell according to the formula:  $(3 * \text{RAND}())^{.333}$  which will yield a random number between 0 and  $3^{1/3}$  with a probability distribution function that varies as the square of y, as shown in Fig A4.

Unfortunately, to obtain a normal distribution is much more difficult. In this

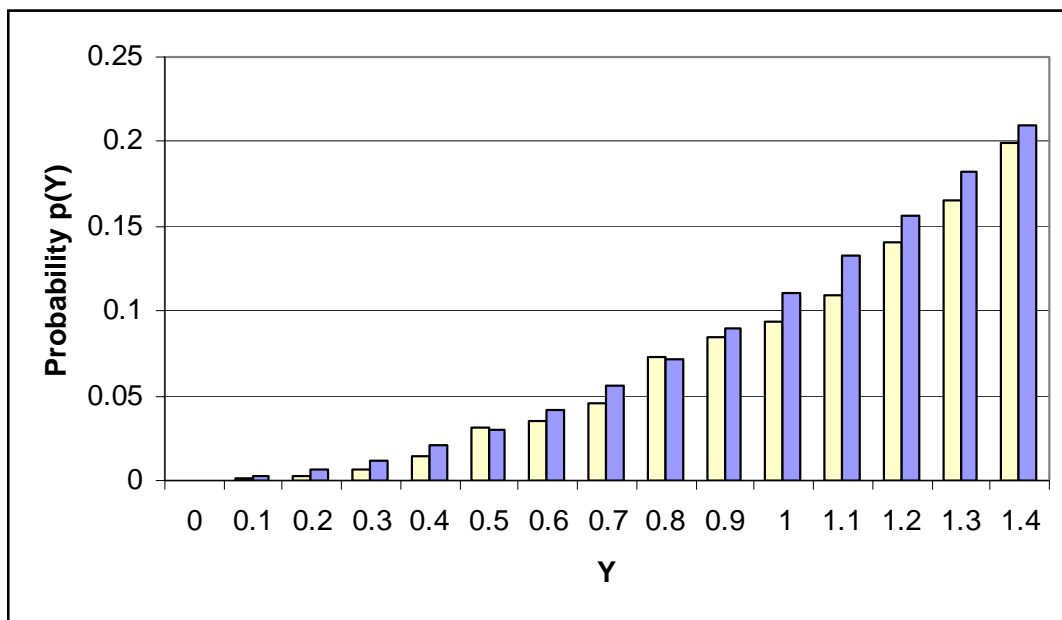


Figure A4. A quadratic probability distribution function. Yellow is the result of 1000 trials, and blue is the theoretical distribution.

work we used an approximate transformation of  $y = 2^{1/2} \ln(x)$  or as implemented in EXCEL:  $\text{LN}(\text{RAND}()+0.0001)*(0.707)*\text{SIGN}(\text{RAND}()-0.5)$ . This distribution has a unity standard deviation, a mean of zero, but does not fall off as rapidly as a normal distribution. An example distribution is shown in FIG A4 compared to the normal distribution.

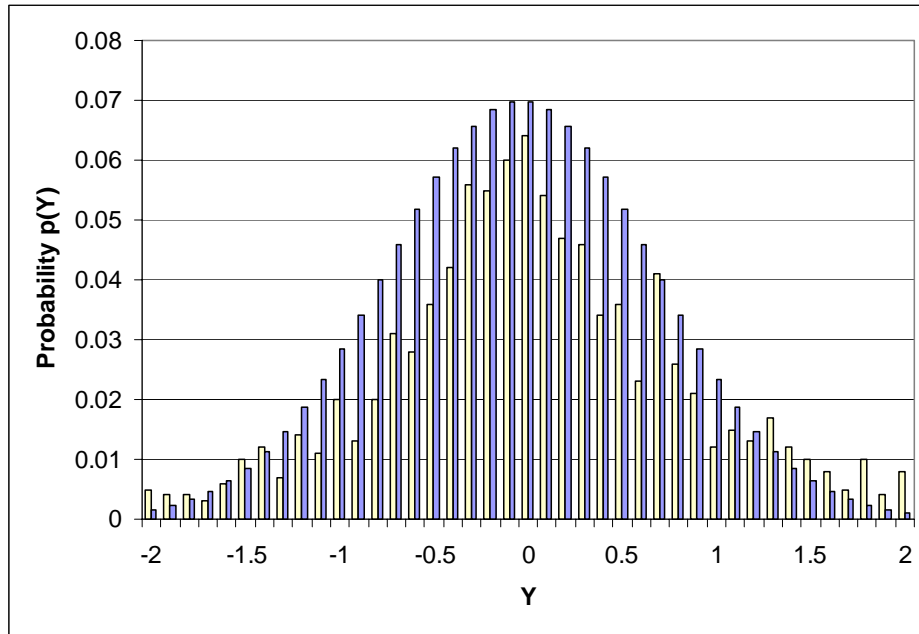


Figure A5. Normal distribution (blue) and pseudo-normal distribution used in Monte-Carlo simulations (yellow). Both have a standard deviation of unity and zero mean.

For the Monte-Carlo simulations, different distribution functions were tried, including a uniform distribution over a limited range, a triangular distribution, and the psuedo-normal distribution. It was found, fortunately but somewhat surprisingly, that the distribution function did not have much effect on the actual noise values generated by the simulation provided the distribution functions had a standard deviation of unity, and mean of zero.

## Acknowledgments

The author appreciates stimulating discussions with his former colleagues at JPL and with his current colleagues at Micron on the topic of noise in CMOS APS devices, including Bedabrata Pain, Tom Cunningham, Gennady Agranov, Vlad Berezin, Alex Krymski, and Sandor Barna.

## References

1. F. Sangster and K. Teer, "Bucket brigade electronics – new possibilities for delay, time-axis conversion, and scanning," *IEEE J. Solid-State Circuits*, vol. 4, pp. 131-136, 1969.
2. W.S. Boyle and G.E. Smith, "Charge coupled semiconductor devices," *Bell Syst. Tech. J.*, vol 49, no. 4, pp. 587-593, 1970.
3. K.K. Thornber, "Noise suppression in charge transfer devices," *Proc. IEEE*, vol. 60, pp. 1113-1114, 1972.
4. K.K. Thornber, "Theory of noise in charge-transfer devices," *Bell Syst. Tech. J.*, vol. 53, no.7 , pp. 1211-1262, 1974.
5. E.R. Fossum, "CMOS image sensors: electronic camera-on-a-chip," *IEEE Trans. Electron Devices*, vol. 44, no. 10, pp. 1689-1698, 1997.
6. P. Lee, R. Gee, M. Guidash, T-H. Lee, and E.R. Fossum, "An active pixel sensor fabricated using CMOS/CCD process technology," presented at the IEEE Workshop on Charge-Coupled Devices and Advanced Image Sensors, Dana Point, California, April 1995.
7. S. Mendis, S. Kemeny, E.R. Fossum, "A 128x128 CMOS active pixel image sensor for highly integrated imaging systems," in *IEEE IEDM Tech. Dig.*, 1993., pp. 583-586.
8. S. Mendis, S. Kemeny, R. Gee, B. Pain, E.R. Fossum, "Progress in CMOS active pixel image sensors," *Charge-Coupled Devices and Solid State Optical Sensors IV, Proc. SPIE*, vol. 2172, pp 19-29, 1994.

9. P. Noble, "Self-scanned silicon image detector arrays," *IEEE Trans. Electron Devices*, vol. 15, pp. 202-209, 1968.
10. R.H. Nixon, S. Kemeny, C. Staller and E.R. Fossum, "128 x 128 CMOS photodiode-type active pixel sensor with on-chip timing, control and signal chain electronics," *Charge-Coupled Devices and Solid-State Optical Sensors V, Proc. SPIE*, vol. 2415, pp. 117-123, 1995.
11. B. Pain, G. Yang, M. Ortiz, C. Wrigley, B. Hancock, T. Cunningham, "Analysis and enhancement of low-light-level performance of photodiode-type CMOS active pixel imagers operated with sub-threshold reset," presented at IEEE Workshop on Charge-Coupled Devices and Advanced Image Sensors, Nagano, Japan, June 1999.
12. H. Tian, B. Fowler, and A. Gamal, "Analysis of temporal noise in CMOS photodiode active pixel sensor," *IEEE J. Solid-State Circuits*, vol. 36, no. 1, pp. 92-101, 2001.
13. G. Agranov, unpublished results, private communication.